




Effect of oxidation time on microstructure and mechanical properties of C_f/SiC–Al composites after high-temperature oxidation

Jiahao Liao^{1,2}, Lixia Yang^{1,*} , Zhaofeng Chen^{1,*}, Tianru Guan¹, and Tianlong Liu¹

¹International Laboratory for Insulation and Energy Efficiency Materials, College of Materials Science and Technology, Nanjing University of Aeronautics and Astronautics, Nanjing 211106, People's Republic of China

²Suzhou Superlong Aviation Heat Resistance Materials Technology Co., Ltd, Suzhou 215400, People's Republic of China

Received: 15 November 2022

Accepted: 21 January 2023

Published online:

4 February 2023

© The Author(s), under exclusive licence to Springer Science+Business Media, LLC, part of Springer Nature 2023

ABSTRACT

The microstructure and elemental composition evolution of C_f/SiC–Al composites prepared by combined precursor infiltration pyrolysis (PIP) and vacuum-pressure infiltration processes after high-temperature oxidation for different times was investigated. Meanwhile, the mechanical properties of the composites after oxidation treatment were characterized by nanoindentation and compressive performance tests. The results show that when the oxidation temperature was 400 °C and above, the weight loss rate of the composites gradually increased with the prolongation of the oxidation time, and the interface separation between the carbon fiber and SiC matrix became more obvious. Moreover, the nanoindentation elastic modulus of the Al alloy matrix and the SiC matrix decreased significantly with the increase in oxidation time, while the nanoindentation hardness of the aluminum alloy hardly changed. After oxidizing at 400 °C for 7 h, the in-plane compressive strength of the composites reached the maximum (584.7 MPa), and after oxidizing at 500 °C for 9 h, the compressive strength decreased to the minimum (347.8 MPa).

Introduction

Continuous carbon fiber-reinforced aluminum matrix (C_f/Al) composites have become the key application materials for the development of high-performance and lightweight aerospace vehicles because of their

performance advantages such as low density, high strength, high modulus, low thermal expansion coefficient and high reliability [1–3]. However, with the expansion of the application range, higher requirements are put forward for the performance of C_f/Al composites, especially the high-temperature resistance [4, 5].

Handling Editor: Catalin Croitoru.

Address correspondence to E-mail: lixiayang@nuaa.edu.cn; zhaofeng_chen@163.com

<https://doi.org/10.1007/s10853-023-08242-8>

For the Al alloy matrix, researchers mainly enhance its high-temperature performance by introducing high melting point metal elements [6, 7] or second phases (ceramic particles, whiskers and nanotubes, etc.) [8–10]. However, for C_f /Al composites, due to the existence of the continuous carbon fiber-reinforced phase, it is difficult for Al alloy modified by the second phase to be melted and infiltrated into the fiber preform due to the limitation of the preparation process. Xu et al. [5] improved the high-temperature resistance of Al-Si alloy by introducing transition metal Fe element, and successfully infiltrated it into unidirectional winding carbon fiber preform to obtain C_f /Al-Fe-Mg-Si composites with excellent high-temperature performance. Nevertheless, such method is only suitable for fiber preforms with simple structure. When the weaving structure of the preform is changed into a three-dimensional woven structure, the modified Al alloy is difficult to effectively infiltrate into the complex preform due to its high melt viscosity. Inspired by the design and preparation ideas of continuous fiber-reinforced ceramic matrix composites (the most promising high-temperature structural composites at present [11–13]), in our previous research, SiC ceramics were in situ composited into preforms by the precursor infiltration pyrolysis (PIP) method and the Al-Si alloy matrix was infiltrated and filled to improve the high-temperature performance of the three-dimensional braided C_f /Al composites [14, 15]. For the successfully prepared C_f /SiC-Al composites, its application goal is mainly to become the key structural material for the medium-high temperature (< 60 °C) bearing parts of aero-engines and launch vehicles. However, the components in this field require high service reliability of materials used in thermal/oxygen environment. Therefore, in order to serve reliably in high-temperature environment, in-depth research on high-temperature performance and oxidation resistance of C_f /SiC-Al composites must be carried out to reveal the evolution law of microstructure and properties of the composites in thermal/oxygen environment. Meanwhile, it is of great significance to accelerate the use of the composites in actual working conditions.

In this study, the evolution of microstructure, elemental composition and mechanical properties of the as-prepared C_f /SiC-Al composites after treatment with different oxidation temperatures and times was

investigated, and the oxidation mechanism and failure mode were also discussed.

Experimental procedure

Material preparation

C_f /SiC-Al composites were reinforced by a three-dimensional needle-stitched carbon fiber (12 K, T700, Toray, Japan) preform, and its fiber volume fraction was about 40%. First, a layer of pyrolytic carbon interface with a thickness of about 0.2–0.3 μm was deposited on the carbon fiber surface by a chemical vapor infiltration process (propylene and Ar gas flow ratio was 1:2, and deposition temperature was 1000 °C). Then, SiC matrix was in situ composited into the fiber preform by the PIP process (polycarbosilane was the ceramic precursor, xylene was the solvent, the weight ratio of the two was 1:1, and the pyrolysis temperature was 1200 °C), and the volume content of SiC matrix was about 35%. Finally, the ZL101A Al alloy was infiltrated into the preform by vacuum-pressure infiltration process (the temperature of the preform during molten Al alloy infiltration was 550 °C, and the nitrogen pressure during infiltration was 1.2 MPa), and the volume fraction of Al alloy matrix was about 22%. A more detailed preparation process and schematic diagram are shown in Ref. [14]. Figure 1 shows the cross-sectional micromorphology and element composition distribution of the as-prepared C_f /SiC-Al composites. The composites have high density and almost no residual large-sized pores (Fig. 1a), the Al alloy is closely bonded to the SiC matrix, and there are no defects and cracks at the interface between the two (Fig. 1b, c). In addition, the interface between the carbon fiber and the SiC matrix is also relatively tightly bound, and there is no interface separation (Fig. 1d).

Test characterization

The long-term oxidation test of the as-prepared C_f /SiC-Al composites at high temperature was carried out in a box furnace (model KF1100, Nanjing by Instrument Technology Co., Ltd.) with dry static air. Raise the temperature of the samples and furnace to 300 °C, 400 °C and 500 °C, respectively, at a heating rate of 10 °C/min, and then maintain it for 3 h, 5 h, 7 h and 9 h, respectively, at each temperature. After

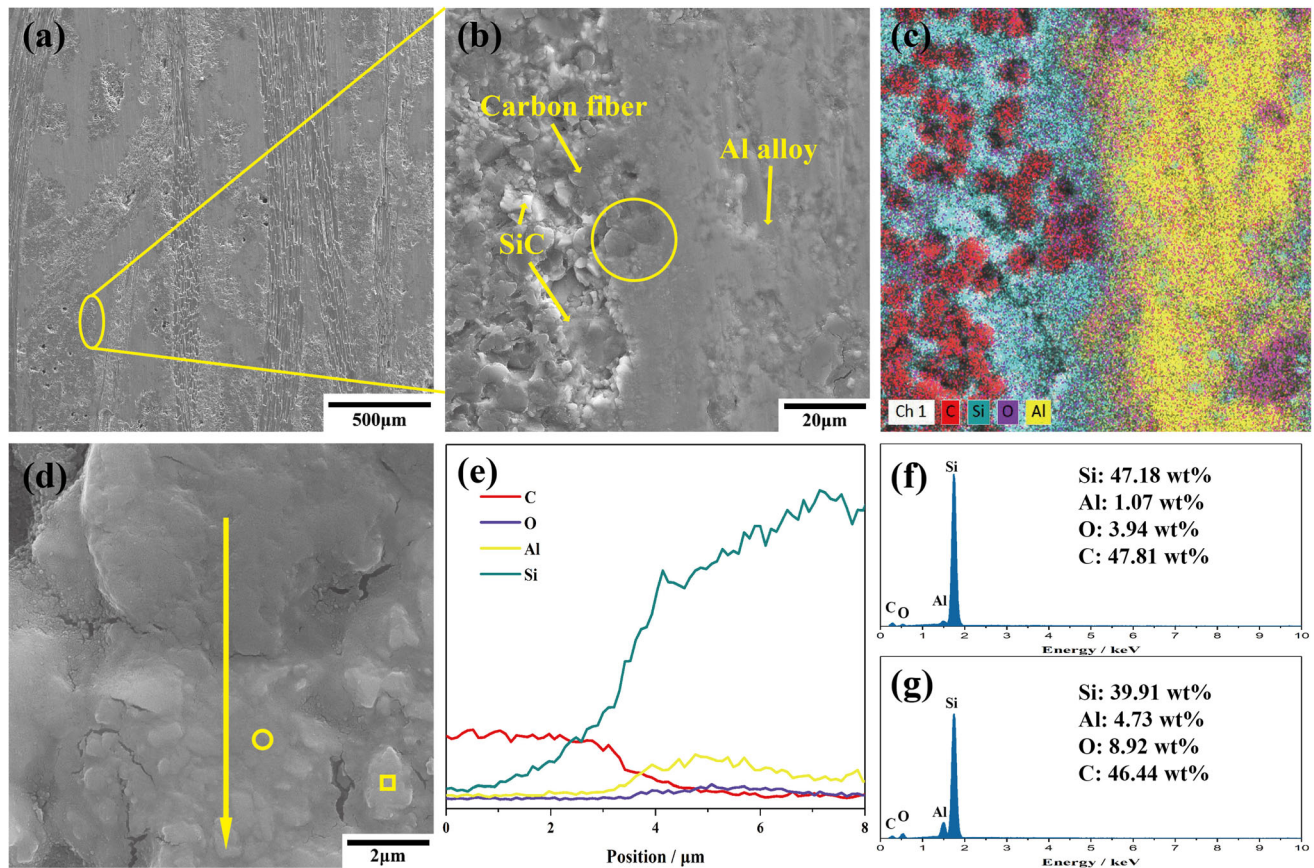


Figure 1 The cross-sectional micromorphology and elemental composition distribution of the as-received composites. **a** and **b** Cross-sectional microstructure, **c** Element mapping of (**b**), **d** Magnification of the yellow circle mark in (**b**), **e** Element line

scanning along the yellow arrows direction in (**b**), **f** Element point scanning marked by yellow squares in (**d**), **g** Element point scans marked by yellow circles in (**d**).

the heat preservation, take out the sample for air cooling. The weight of the samples before and after the oxidation test was weighed by an electronic analytical balance (model hz-224/45, accuracy 0.1 mg, Huazhi scientific instrument). Nanoindentation tests (Bruker Hysitron TI980, Berkovich indenter) were performed at room temperature with a loading/unloading rate of 10 mN/min. The maximum test load is 5mN, and the load was maintained for 10 s after reaching the maximum. According to the load-indentation depth curve, the elastic modulus and nanoindentation hardness were calculated by the Oliver & Pharr method. Figure 2 shows schematic diagram of nanoindentation test of the sample and the distribution of indentation points. The in-plane compressive strength tests of the samples after oxidation test were carried out by an electronic universal testing machine (CMT5205, the maximum load of the sensor is 100 kN) with a displacement loading rate of

0.5 mm/min. And the size of samples for oxidation test and in-plane compressive strength test was $8\text{mm}^L \times 8\text{mm}^W \times 9\text{mm}^H$. Microscopic morphology of the composites was characterized by a scanning electron microscope (SEM, ZEISS Sigma 300, with a Zeiss Smart EDX) and high-resolution transmission electron microscopy (HRTEM, FEI Talos F200X G2). The sample slices for HRTEM observation were prepared by focused ion beam (FIB) technology (FEI Scios 2 HiVac, W as sealing protective layer for ion beam etching of the sample). And the crack and fracture morphologies of the samples after compression test were observed by optical microscope (Nikon SMZ745T, with a RH-XCAM4K8MPA) and scanning electron microscope (TESCAN LYRA3, with a Bruker EDS).

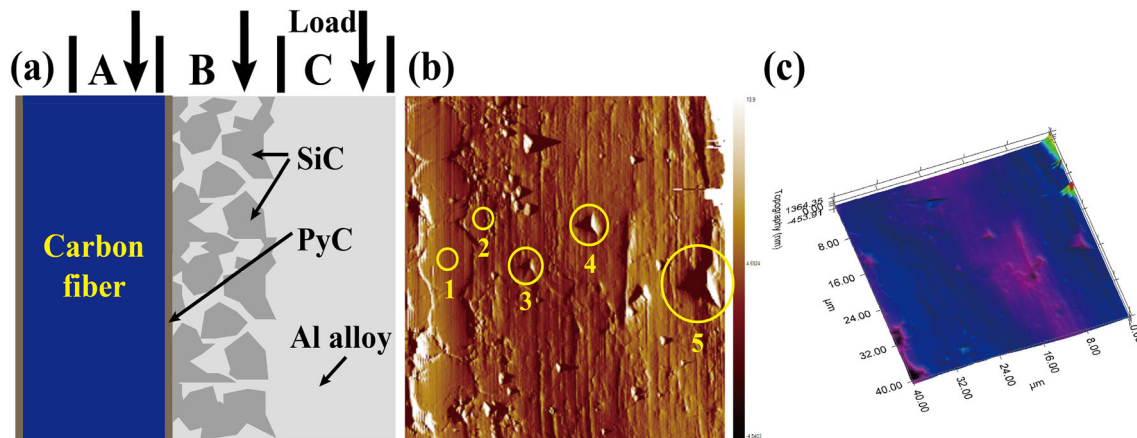


Figure 2 Schematic diagram of nanoindentation test of the sample. **a** Schematic diagram of nanoindentation, **b** Distribution and micromorphology of nanoindentation points, **c** Depth nephogram of nanoindentation point.

Results and discussion

Microstructure and elemental composition evolution after oxidation

The surface microstructure and elemental composition of the as-prepared $C_f/SiC-Al$ composites evolved after being oxidized at different temperatures and for different times, accompanied by weight gain and weight loss. Figure 3 shows the weight change curve of the sample after oxidation treatment. At different oxidation temperatures, the change trend of the sample weight with the prolongation of oxidation time is not consistent. When oxidized at 300 °C, with the prolongation of oxidation time, the sample first loses weight and then gains weight. Then

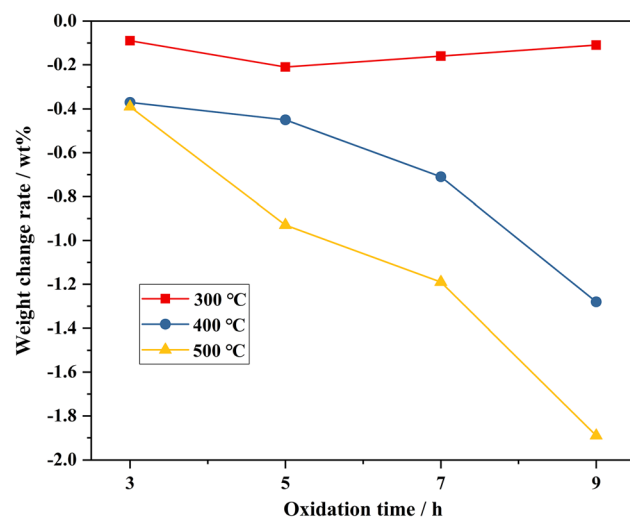
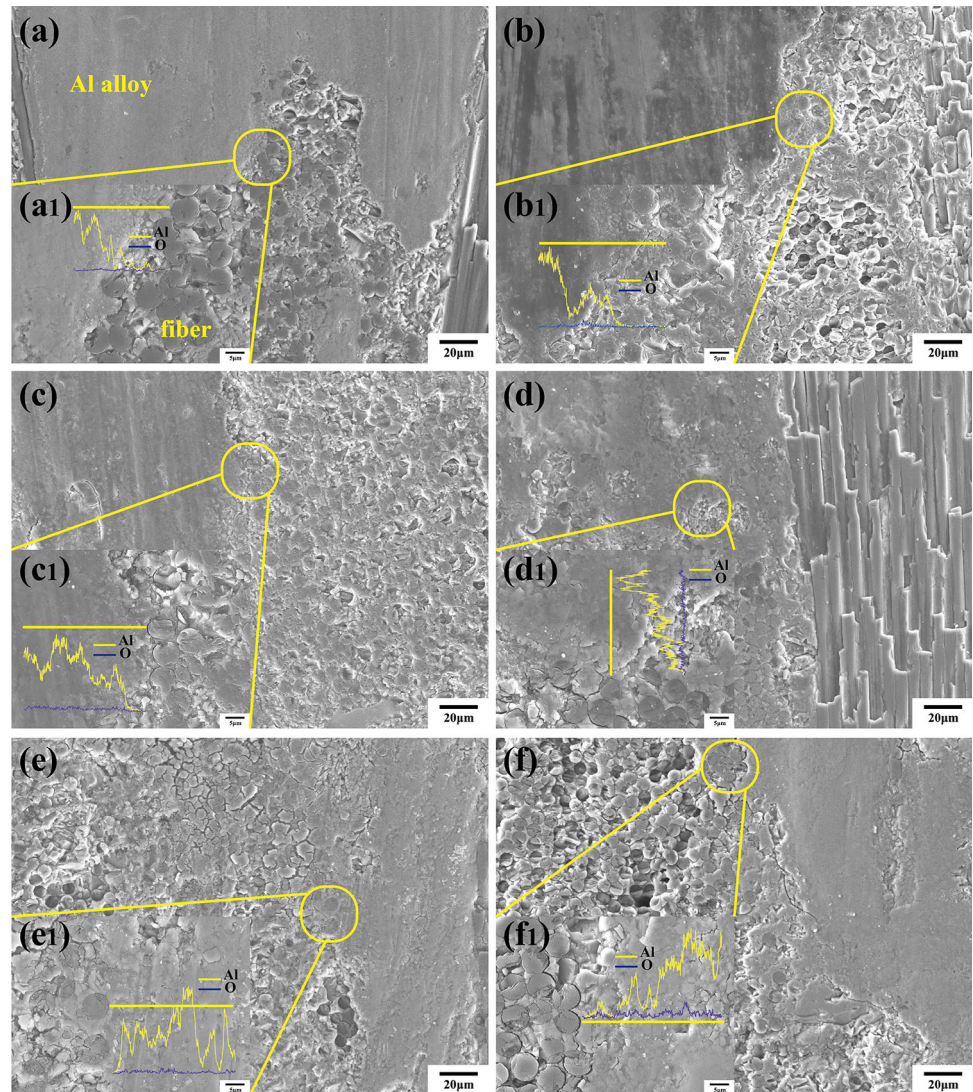


Figure 3 The weight change of the sample with prolonged oxidation time at different temperatures.

after the oxidation temperature is increased to 400 °C and above, the weight of the samples gradually decreases with the prolongation of oxidation time. However, the weight reduction trend is slightly different. At 400 °C, the degree of weight reduction of the sample is more obvious with the prolongation of oxidation time, while at 500 °C, the degree of weight reduction of the sample decreases first and then increases.

Figure 4 shows the microstructures of the samples after oxidation at different temperatures for 5 h and 9 h, respectively. After oxidation at 300 °C for 5 h and 9 h, respectively, the microstructure of the surface of the composites hardly changes compared with that before oxidation (Fig. 4a, b), the carbon fiber and SiC matrix are not eroded by oxidation, and the oxygen element line scan peak of the Al alloy matrix slightly increases (Fig. 4a₁, b₁), which may mean that the thickness of the oxide film on the surface of Al alloy matrix increases with the prolongation of the oxidation time [16]. This may also be the reason for the weight gain of the composites with increasing oxidation time (≥ 5 h) at this temperature. After being oxidized at 400 °C and 500 °C for 5 h and 9 h, respectively, the Al alloy matrix in the composites has not suffered obvious damage due to the existence of oxide film (Fig. 4c–f), but the oxidation damage degree of carbon fiber becomes more serious with the increase in oxidation temperature and the prolongation of oxidation time (Fig. 4c₁–f₁). Figure 5 shows the microstructure and element composition distribution of the Al alloy-SiC matrix-carbon fiber bonding area in $C_f/SiC-Al$ composites after oxidation

Figure 4 Microstructure and element line scans of C_f/SiC–Al composites after oxidation at different temperatures and for different times. **a** and **a**₁ 300 °C–5 h, **b** and **b**₁ 300 °C–9 h, **c** and **c**₁ 400 °C–5 h, **d** and **d**₁ 400 °C–9 h, **e** and **e**₁ 500 °C–5 h, **f** and **f**₁ 500 °C–9 h.



treatment. There is no crack or separation at the interface between the Al alloy and SiC matrix (Fig. 5a–f), although their thermal expansion coefficients are quite different [17, 18], and even the bonding state is improved (Fig. 5f, f₂). It is speculated that the long-term high-temperature environment promotes the diffusion of Si element in the Al alloy matrix to the SiC matrix, and the degree of interface reaction between Al and SiC matrix gradually increases [19, 20]. Since the SiC matrix generated by PIP process can only have obvious oxidation and weight gain at above 800 °C [21], the SiC matrix in the composites has not appeared obvious oxidation erosion after long-term oxidation at 300–500 °C. However, the carbon fibers suffer from oxidative erosion and structural damage, and the damage degree gradually increases with the elevating of temperature

and the prolongation of the oxidation time (Fig. 5a₂–f₂). At 300 °C, the degree of oxidative damage of carbon fibers is low, and the microstructure of the cross-section has not suffered obvious damage, but cracks begin to appear at the fiber/matrix junction, and interface separation occurs. And with the prolongation of oxidation time, the degree of interface separation has not increase significantly (Fig. 5a₂–b₂). At 400 °C, the oxidative damage of carbon fibers aggravates with the prolongation of oxidation time (Fig. 5c₂–d₂). At 500 °C, the degree of oxidative damage of carbon fibers is further aggravated, and with the prolongation of oxidation time, the degree of surface structure damage and interface separation also increases significantly (Fig. 5e₂–f₂).

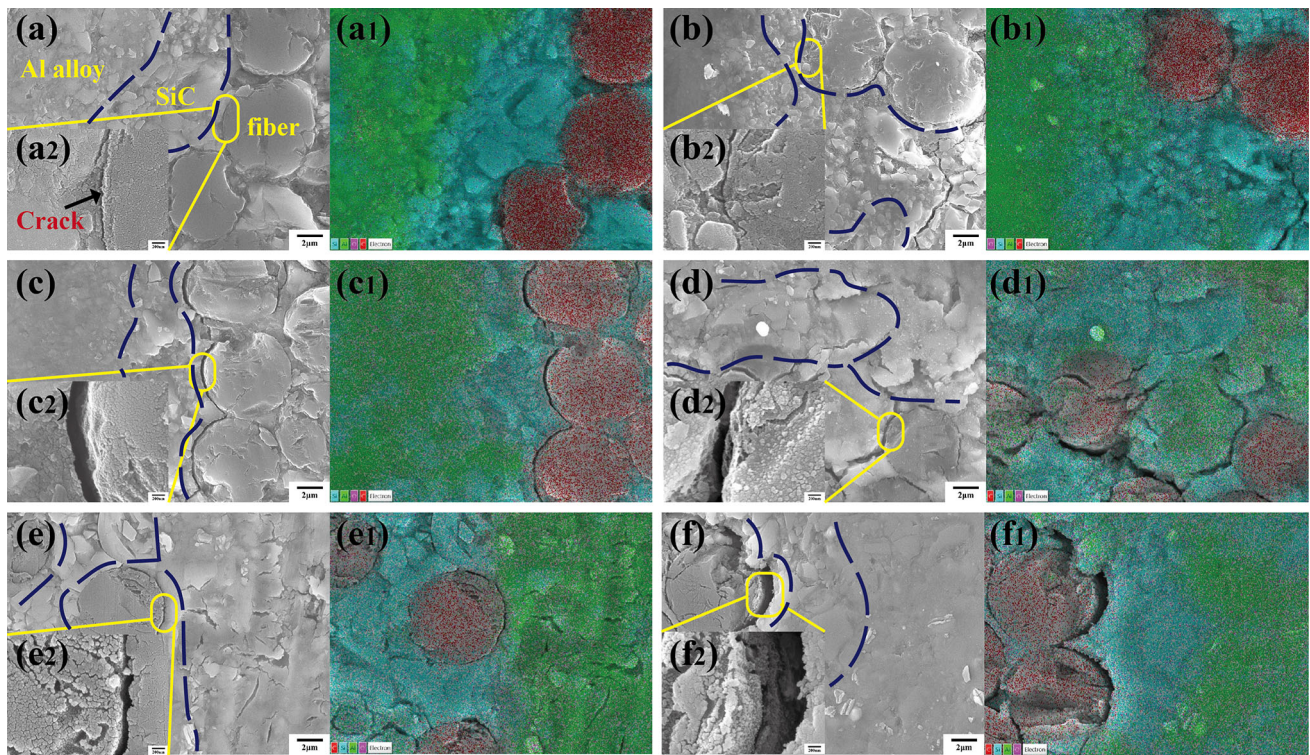


Figure 5 Microstructure and element mapping analysis of carbon fiber and Al alloy matrix bonding area after oxidation. **a**, **a₁** and **a₂** 300 °C-5 h; **b**, **b₁** and **b₂** 300 °C-9 h; **c**, **c₁** and **c₂** 400 °C-5 h; **d**, **d₁** and **d₂** 400 °C-9 h; **e**, **e₁** and **e₂** 500 °C-5 h; **f**, **f₁** and **f₂** 500 °C-9 h.

Nanoindentation performance analysis

The nanoindentation properties of the as-received C_f/SiC–Al after oxidation at different temperatures for 5-h and 9-h composites were characterized. The nanoindentation force–depth curves of each component region of the composites after oxidation treatment are shown in Fig. 6. After 5-h and 9-h oxidation, the maximum depth and residual depth of nanoindentation in Al alloy matrix gradually decreased with the elevating of oxidation temperature. In addition, after 5-h oxidation, the creep displacement of the Al alloy matrix in the holding pressure stage hardly changed with the elevating of oxidation temperature (Fig. 6a, c, e), while after 9-h oxidation, the creep displacement gradually decreased (Fig. 6b, d, f). After oxidation at 300 °C (Fig. 6a, b), the maximum depth of nanoindentation in the Al alloy matrix increased with the prolongation of oxidation time, but the residual depth decreases slightly. After oxidation at 400 °C (Fig. 6c, d), both the maximum depth of nanoindentation and the residual depth of the Al alloy matrix increased significantly with the prolongation of oxidation time. After oxidation at 500 °C (Fig. 6e, f), the maximum depth of

nanoindentation in the Al alloy matrix hardly changed with the prolongation of oxidation time, but the residual depth decreased slightly. After 5-h and 9-h oxidation, the maximum depth of nanoindentation of carbon fibers (with almost no residual depth) gradually increased with the elevating of temperature. At the same oxidation temperature, the maximum depth of nanoindentation of carbon fibers has not changed significantly with the elevating of oxidation temperature. However, after 9-h oxidation, the creep displacement of carbon fibers in the holding pressure stage gradually increased with the elevating of oxidation temperature. After 5-h oxidation, the maximum depth of nanoindentation of the SiC matrix hardly changed with the elevating of oxidation temperature, and there was no obvious creep stage. After 9-h oxidation, the maximum depth of nanoindentation in the SiC matrix gradually increased with the elevating of temperature, and creep occurred in all of them. In the SiC–Al alloy bonding zone, the closer to the SiC matrix, the smaller the nanoindentation depth, and the greater the closer to the Al alloy.

The elastic modulus of each component region of the composites after oxidation treatment is shown in

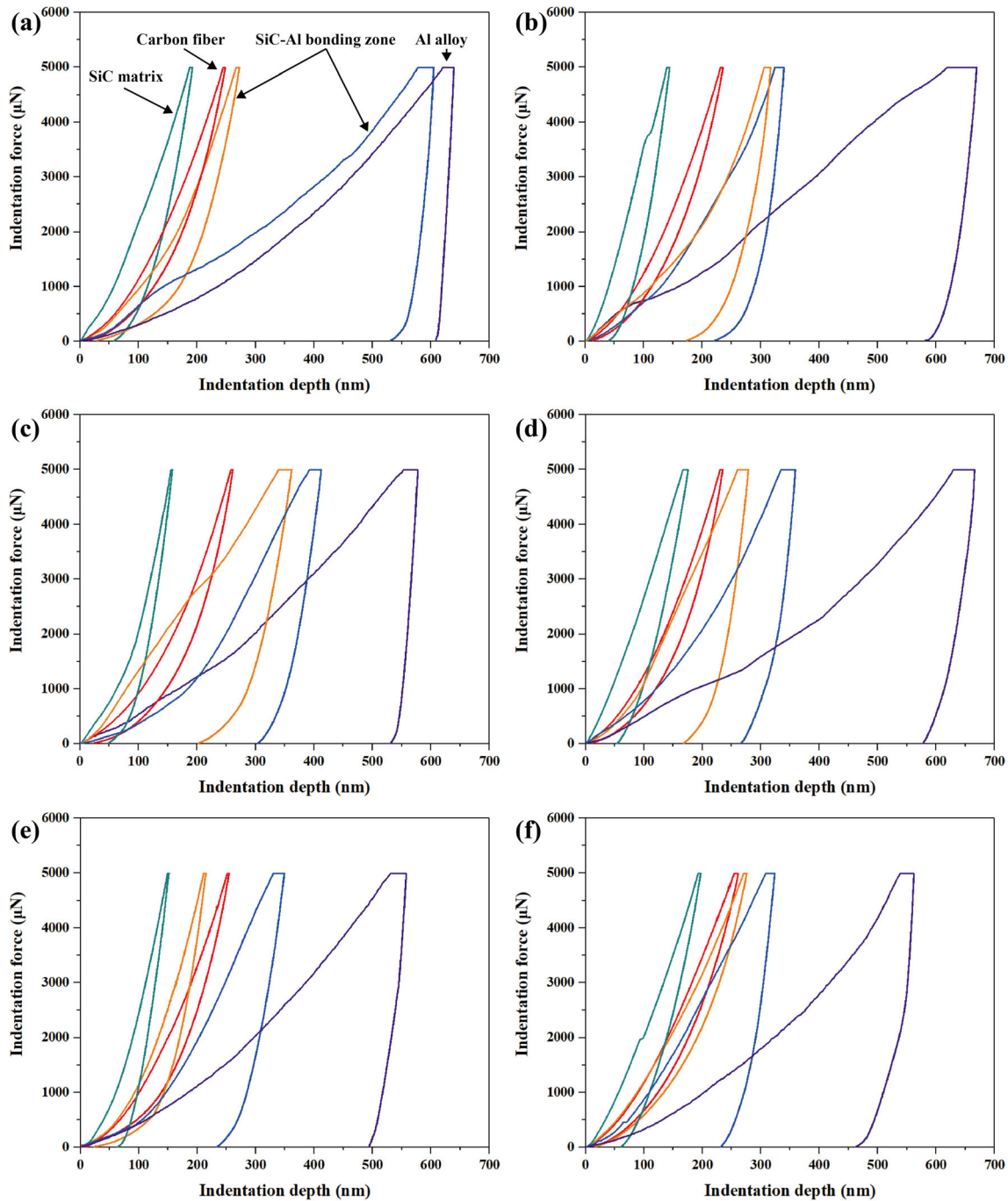


Figure 6 Nanoindentation force–depth curves of each component region of the composites oxidized in high-temperature air environment for different times. **a** 300 °C-5 h, **b** 300 °C-9 h; **c** 400 °C-5 h, **d** 400 °C-9 h; **e** 500 °C-5 h, **f** 500 °C-9 h.

Fig. 7. After 5 h of oxidation (Fig. 7a), with the elevating of oxidation temperature, the elastic modulus of the Al alloy matrix gradually decreased (from 53.1 to 41.3 GPa), the elastic modulus of the SiC matrix increased slightly (from 112.7 to 116.9 GPa), the elastic modulus of carbon fiber has almost no changed, and the elastic modulus of the SiC–Al alloy

bonding area first decreased and then increased. After the oxidation time increased to 9 h (Fig. 7b), with the elevating of temperature, the elastic modulus of the Al alloy matrix first decreased and then increased, and the elastic modulus of the SiC matrix decreased significantly (from 113.2 to 65.3 GPa). The elastic modulus of carbon fiber first increased slightly

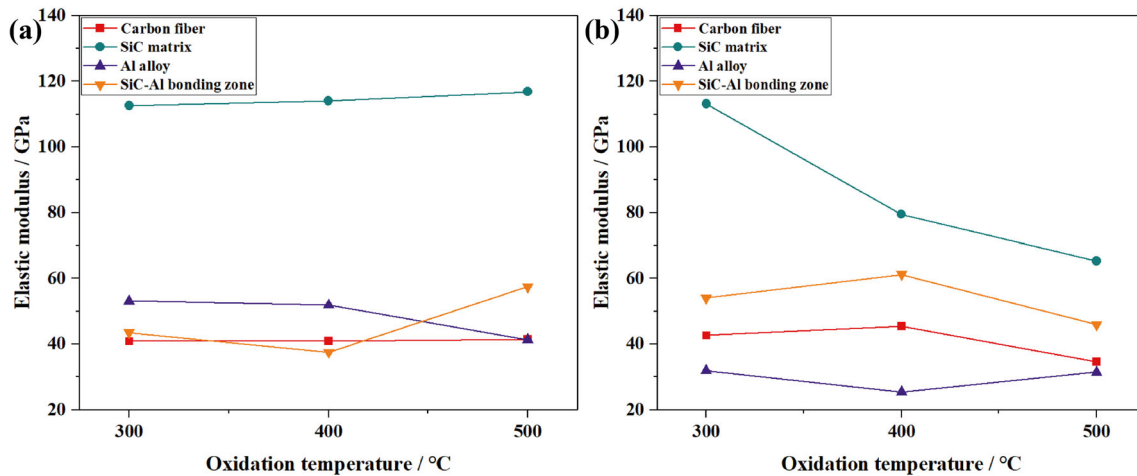


Figure 7 Nanoindentation elastic modulus of each component region of the composites oxidized in high-temperature air environment for different times. **a** Oxidized for 5 h; **b** Oxidized for 9 h.

and then decreased significantly (the minimum value was 34.6 GPa after oxidation at 500 °C), and the elastic modulus of the SiC–Al alloy bonding region first increased and then decreased, similar to carbon fiber. In addition, at the same oxidation temperature, the elastic modulus of the Al alloy matrix decreased with the prolongation of oxidation time. The elastic modulus of the SiC matrix decreased with the prolongation of the oxidation time after the oxidation temperature reached 400 °C. Figure 8 shows the nanoindentation hardness of each component region of the composites after oxidation treatment. After 5 h of oxidation (Fig. 8a), the nanoindentation hardness of the Al alloy matrix increased slightly (from 0.37 to 0.49 GPa) with the elevating of temperature. The

nanoindentation hardness of the SiC matrix first decreased and then increased, and the carbon fiber and SiC–Al alloy bonding areas were similar. After the oxidation time increased to 9 h (Fig. 8b), the nanoindentation hardness of the Al alloy matrix increased slightly (from 0.34 to 0.49 GPa) with the elevating of temperature, while the nanoindentation hardness of the SiC matrix and carbon fiber gradually decreased. And the nanoindentation hardness of the SiC–Al alloy bonding region increased gradually. In addition, at the same oxidation temperature, the nanoindentation hardness of the Al alloy matrix hardly changed with the prolongation of oxidation time. The nanoindentation hardness of the SiC matrix decreased with the prolongation of the oxidation time

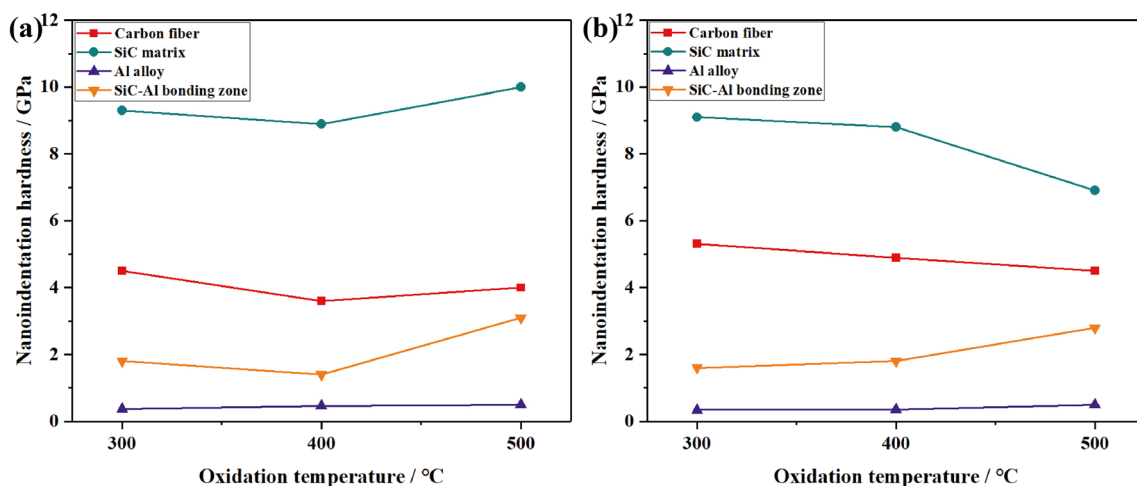


Figure 8 Nanoindentation hardness of each component region of the composites oxidized in high-temperature air environment for different times. **a** Oxidized for 5 h; **b** Oxidized for 9 h.

only after the temperature reached 500 °C, and the nanoindentation hardness of the carbon fiber increased instead.

Evolution of mechanical properties

Figure 9 shows the in-plane compressive stress-displacement curves of the composites after being oxidized at high temperature for different times, as well as the comparative analysis of the compressive strength. At different oxidation temperatures (300 °C, 400 °C and 500 °C), the in-plane compressive stress-displacement curves of the composites after different oxidation times (3 h, 5 h, 7 h and 9 h) are roughly divided into three stages (Fig. 9a): (I) The elastic modulus gradually increases with increasing load

(the curve is nonlinear); (II) the linear segment with stable elastic modulus; (III) the staircase point occurs with further increasing load, and finally a non-brittle fracture occurs. In stage I, with the increase in the compressive load, the residual pores inside the composites are squeezed and closed [22]. At the same time, the Al alloy matrix first undergoes a certain degree of plastic deformation due to the low elastic modulus [23], resulting in the gradual increase of elastic modulus. In stage II, since the residual pores in the composites have been closed, and the load is transferred to the carbon fiber through the matrix, the components are uniformly loaded, and the elastic modulus of the composites hardly changes. In stage III, when the load increases to the critical point of the bearing capacity of the matrix, the matrix begins to

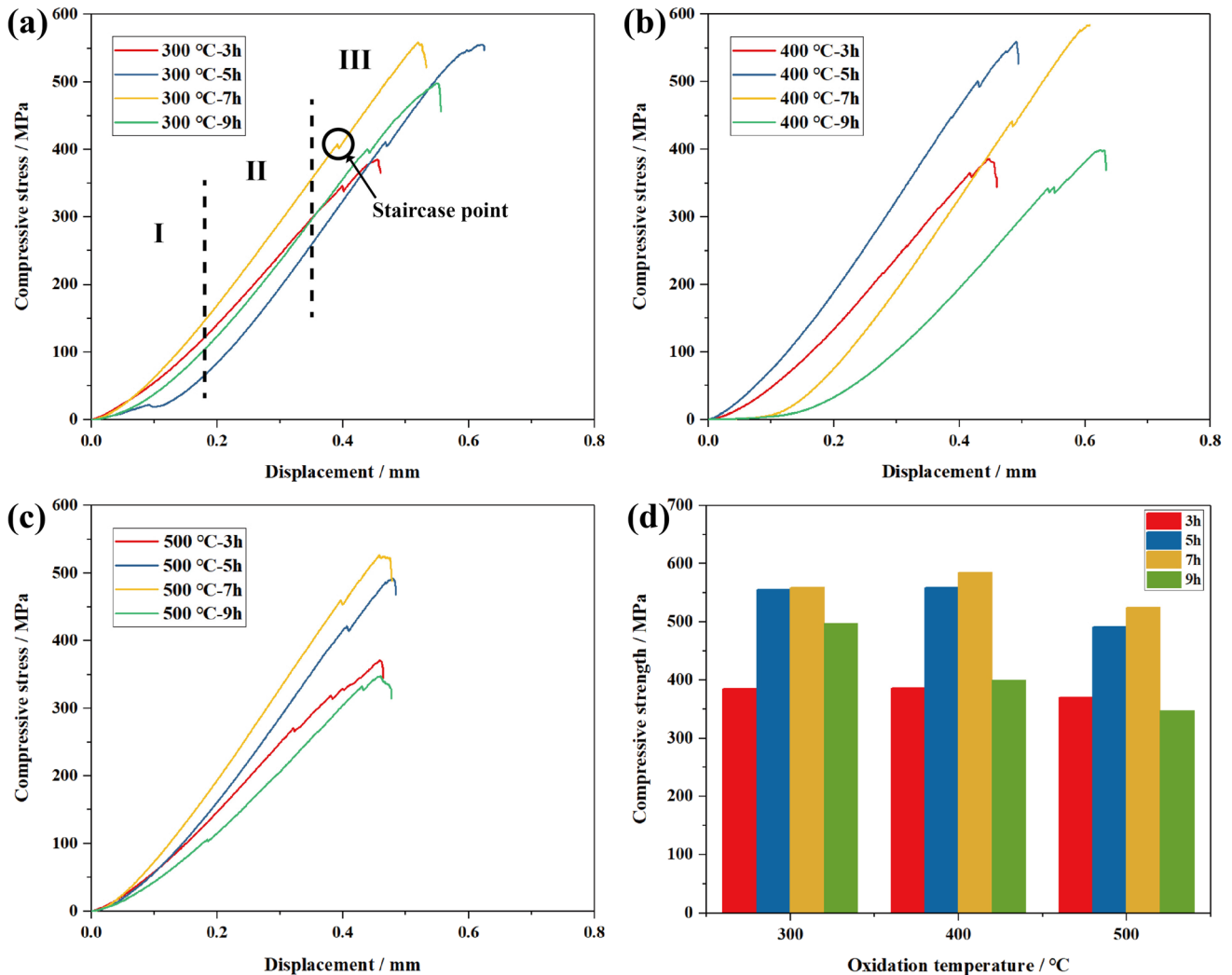


Figure 9 In-plane compressive stress-displacement curves and compressive strength of the composites oxidized at different temperatures for different times. **a** 300 °C-3 ~ 9 h; **b** 400 °C-3 ~ 9 h; **c** 500 °C-3 ~ 9 h; **d** Compressive strength comparison.

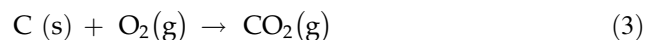
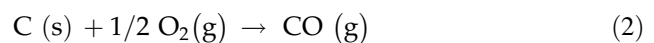
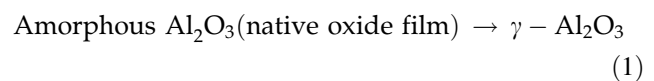
produce microcracks, but as the load increases, the microcracks are squeezed and closed, resulting in the staircase point [24]. Finally, with the further increase in the load, microcracks re-initiated in the matrix and gradually accumulated and expanded, and finally macrocracks occurred through the fibers, leading to the failure of the composites [22, 25]. At each oxidation temperature, the in-plane compressive strength of the composites first increased and then decreased with the prolongation of oxidation time (the maximum after 7 h of oxidation, as shown in Fig. 9d). After oxidation for 3 h, 5 h and 7 h, respectively, the compressive strength of the composites first increased slightly and then decreased with the increase in the oxidation temperature. And the compressive strength gradually decreased after 9-h oxidation. At the oxidation temperature of 500 °C, the compressive strength after 9-h oxidation is less than that after 3-h oxidation; the main reason should be that the damage degree of carbon fiber reaches the maximum. In addition, after oxidation at 500 °C, the fracture displacement of the composites is the smallest (Fig. 9c), especially with the prolongation of oxidation time, the fracture displacement is significantly smaller than that of other oxidation temperatures.

The macrocracks after the compressive performance test of the composites are shown in Fig. 10. As the oxidation temperature at 300 °C, the crack propagation paths of the composites after oxidation for 5 h are obviously more than those after oxidation for 9 h, and the number of crack deflection branches is also more (Fig. 10a, d). This should also be the main reason for the larger fracture displacement of the composites after 5-h oxidation (Fig. 9a). As the oxidation temperature at 400 °C, the crack propagation direction of the composites after 5-h oxidation is roughly along 45° and directly penetrates the material (Fig. 10b). After 9 h of oxidation, the main crack expands for a certain distance and then bifurcates into two sub-cracks (Fig. 10e), thus making the fracture displacement of the composites larger (Fig. 9b). As the oxidation temperature at 500 °C, the main cracks directly penetrate the entire material along the 45° direction after the composites are oxidized for 5 h and 9 h, respectively (Fig. 10c, f), so that the fracture displacement is almost the same (Fig. 9c). Figure 11 shows the microstructure of the compression fracture of the composites. As the oxidation temperature at 300 °C, the number of fibers pulled out at the fracture

of the composites after oxidation for 5 h is significantly more than that after oxidation for 9 h (Fig. 11a, d), and the pull-out length is also longer (Fig. 11a₁, d₁), which is the main reason that the macrocracks are more prone to deflection. At the oxidation temperature of 400 °C, the fiber pull-out at the fracture of the composites after oxidation for 9 h is more obvious (Fig. 11e), and the pull-out length is also longer (Fig. 11e₁). At the oxidation temperature of 500 °C, the fibers at the fracture of the composites are pulled out mainly in bundles (Fig. 11c, f), and more matrix is adhered (Fig. 11c₁, f₁), resulting in less deflection of macrocracks.

Oxidation mechanisms

In a high-temperature (≤ 500 °C) and dry air environment, the microstructure and composition of each component region of the as-received C_f/SiC–Al composites mainly undergo the following evolutions (as shown in Fig. 12): (I) An oxide film was formed on the surface of the Al alloy matrix; (II) carbon fibers suffered from oxidative erosion, and the microstructure was destroyed; (III) the surface of SiC matrix was oxidized to form an oxide film. The main chemical reactions are as follows [19, 26, 27]:



At room temperature, an amorphous Al₂O₃ film can naturally form on the surface of the Al alloy matrix [28]. As the oxidation temperature increased, amorphous Al₂O₃ gradually transforms into crystalline γ -Al₂O₃ (starting at 400 °C and complete transformation at 500 °C, as shown in Reaction (1)) [16]. This should be the main reason for the slight gradual increase in the nanoindentation hardness of the Al alloy matrix with the elevating of the oxidation temperature. Figure 13 shows the HRTEM micrographs of the oxide film formed on Al alloy in the C_f/SiC–Al composites after oxidation at 300 °C and 500 °C for 9 h, respectively. It can be seen that the oxide film has changed from amorphous Al₂O₃ to γ -Al₂O₃ with the increase in oxidation temperature, consistent with the research results in the literature

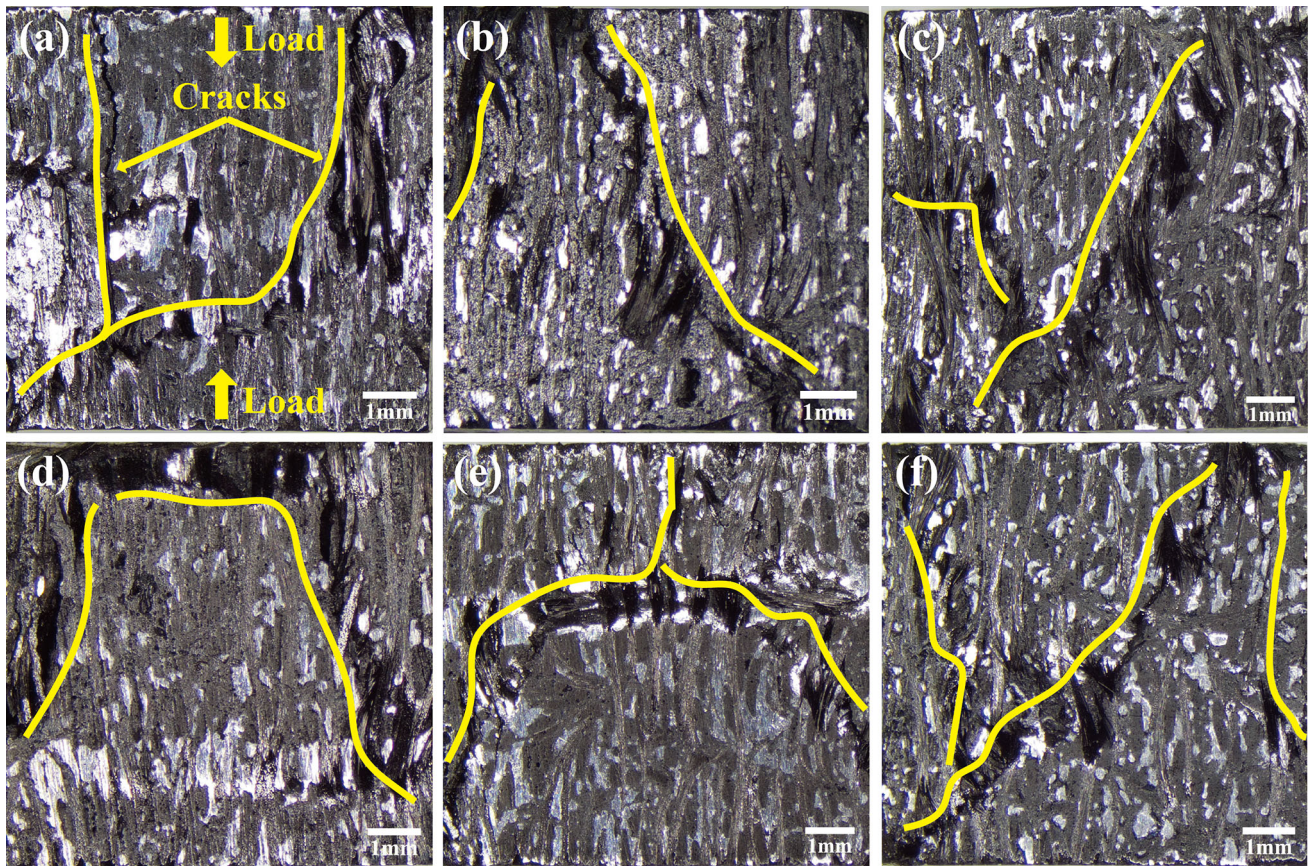


Figure 10 Compressive macrocracks in the composites after oxidation treatment. **a** 300 °C-5 h, **b** 400 °C-5 h, **c** 500 °C-5 h; **d** 300 °C-9 h, **e** 400 °C-9 h, **f** 500 °C-9 h.

[16, 26], and the thickness has also been nearly doubled. In addition, the literature [16] shows that even at the same temperature, the thickness of the oxide film can gradually increase with the prolongation of oxidation time. Under the high-temperature aerobic environment, the mass loss of carbon fiber mainly comes from the carbon–oxygen reaction (Reactions (2) and (3)). Nakamura et al. reported [29] that the weight loss of vapor-grown carbon fibers was 1.7 wt% after oxidation at 400 °C in dry air for 24 h. As the temperature was increased to 500 °C, the oxidation weight loss reached 4.7 wt%, and the carbon fiber structure was severely damaged. Li et al. reported [30] the TG-DSC curve of T700 carbon fiber and found that when the temperature reached 350 °C, the fiber began to lose weight by oxidation. Therefore, after the C_f/SiC–Al composites were oxidized at 300 °C, the mass loss first increased and then decreased gradually with the prolongation of the oxidation time. The essential reason should be that on the one hand, the carbon fiber was only slightly

oxidized, and on the other hand, the thickness of the oxide film on the surface of the Al alloy matrix gradually increased. As the temperature reached 400 °C, the oxidation weight loss of carbon fibers increased due to oxidative attack and microstructure damage. Although the crystallinity and thickness of the oxide film on the surface of the Al alloy matrix increased, the oxidation weight loss of the composites gradually increased with the prolongation of oxidation time. After being oxidized at a temperature below 1200 °C, the surface of SiC can be oxidized to form an amorphous SiO₂ film (Reactions (4)) [31, 32]. For the SiC matrix generated by the PIP process, with the elevating of temperature (< 600 °C), the SiC matrix exhibited a slight weight loss due to the existence of residual-free carbon phase [21]. When the temperature exceeded 800 °C, the weight of the SiC matrix gradually increased due to the intensified surface oxidation. Therefore, as temperature ≤ 400 °C, the nanoindentation hardness of the SiC matrix in the composites hardly changed with the

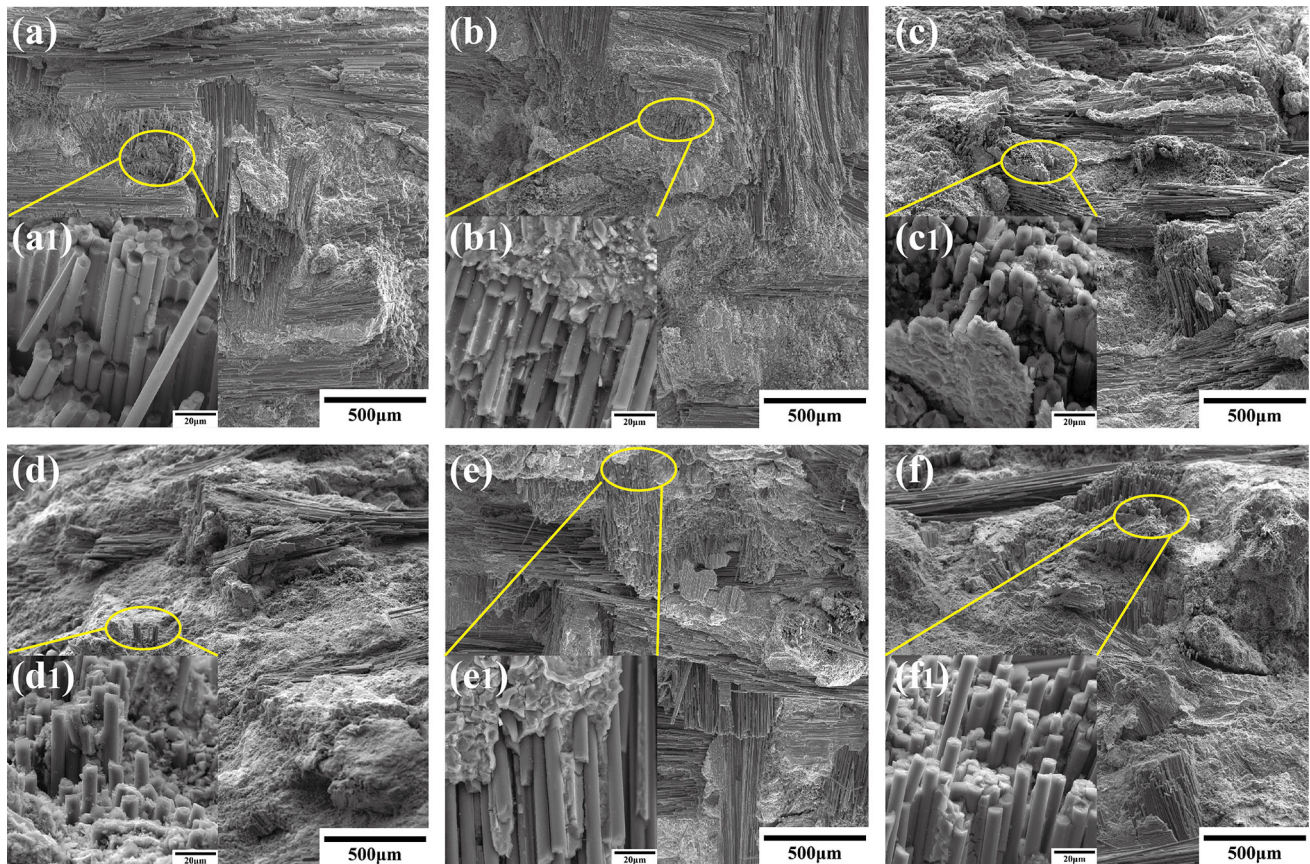


Figure 11 Compression fracture micromorphology of the composites after oxidation treatment. **a** and **a₁** 300 °C-5 h, **b** and **b₁** 400 °C-5 h, **c** and **c₁** 500 °C-5 h; **d** and **d₁** 300 °C-9 h, **e** and **e₁** 400 °C-9 h, **f** and **f₁** 500 °C-9 h.

prolongation of oxidation time (the degree of surface oxidation was lower). As the oxidation temperature at 500 °C, the nanoindentation hardness and elastic modulus of the SiC matrix decreased with the prolongation of the oxidation time, which is inferred that the oxidation degree of the SiC matrix intensified and the thickness of the oxide film increased [33, 34].

Furthermore, when the oxidation temperature was closed to the solution temperature of the Al-Si alloy (450~550 °C), with the prolongation of the oxidation time, the atoms such as Si and Mg in the Al alloy matrix diffused and migrated to the SiC matrix, which increased the thickness of the interface reaction layer between Al alloy and SiC matrix [19, 33, 35]. Figure 14 shows the HRTEM micrographs of a cross-section of Al alloy-SiC matrix interface bonding area in the C_f/SiC-Al composites after oxidation at 500 °C for 9 h. It can be seen that there are many Si enrichment areas et al. alloy-SiC matrix interface bonding area, and there is an obvious diffusion region at the interface between the Si

enrichment area and the SiC matrix, which is consistent with the conclusions in the references. Moreover, it is worth noting that there is almost no Al₄C₃ brittle phases formed at the interface between the Al alloy and SiC matrix (as shown in Fig. 14a, c) due to the oxidation temperature is lower than 627 °C [36]. Therefore, after the C_f/SiC-Al composites were oxidized at 500 °C, due to the damage of the carbon fiber and the interface separation of carbon fiber-SiC matrix, the cracks mainly propagated along the fiber-SiC matrix interface, and the number of crack deflections in the matrix and the fiber decreased, and finally a rapid fracture occurred.

Conclusions

In this work, the microstructure, elemental composition and mechanical properties of C_f/SiC-Al composites prepared by PIP and vacuum-pressure infiltration processes after being oxidized at different

Figure 12 Evolution of microstructure and composition of the as-received $C_f/SiC-Al$ composites after oxidation at different temperatures for different times.

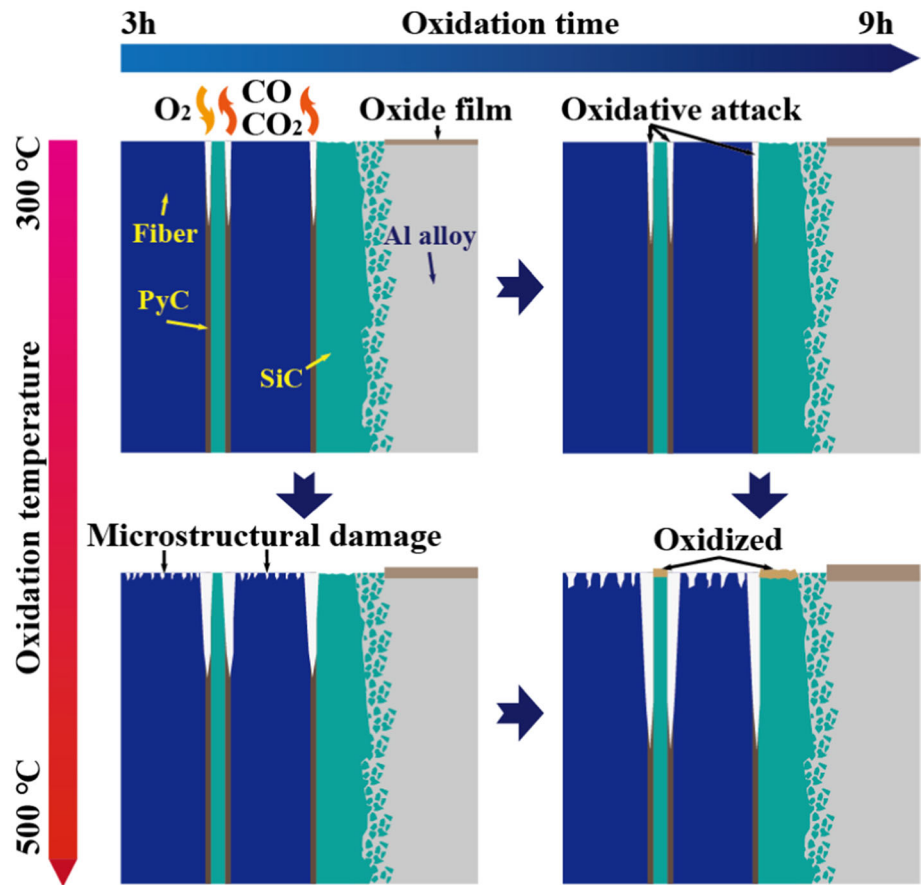
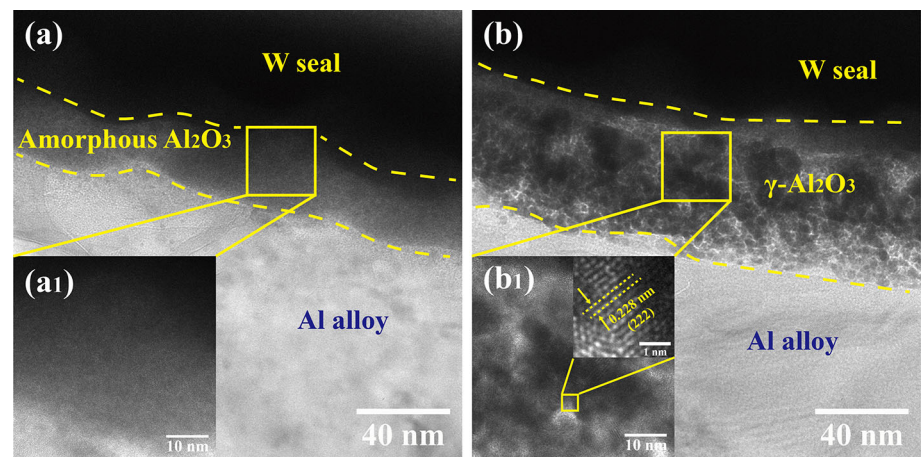


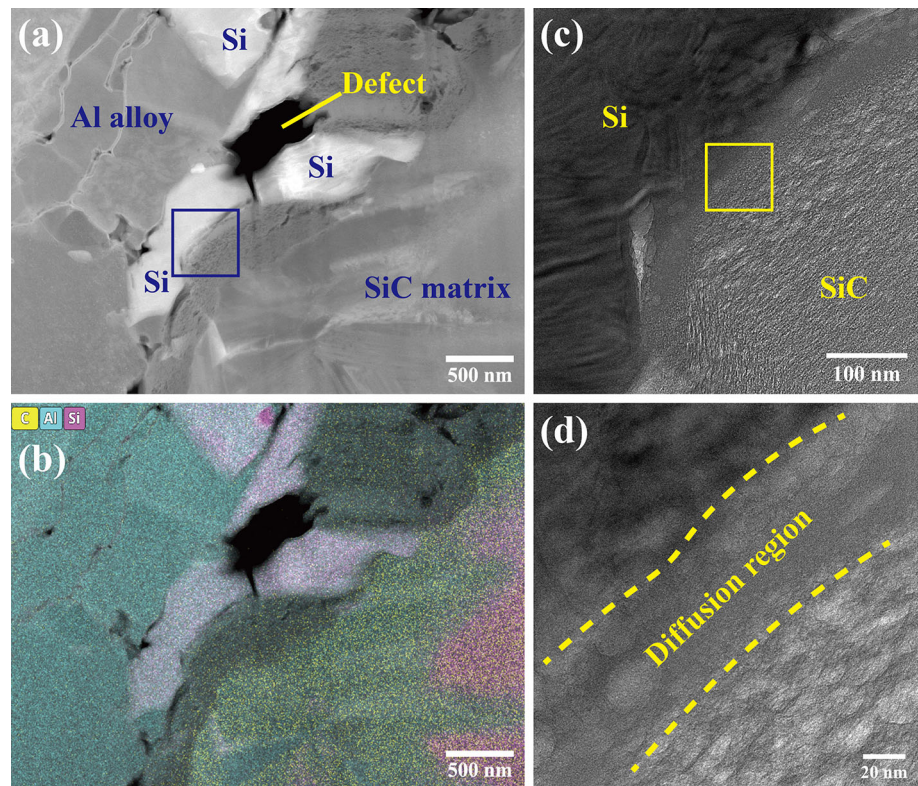
Figure 13 HRTEM micrographs of a cross-section of the oxide film formed on the Al alloy in the $C_f/SiC-Al$ composites after oxidation at different temperatures and for different times. **a** and **a₁** 300 °C-9 h, **b** and **b₁** 500 °C-9 h.



temperatures and for different times were investigated. The main conclusions are as follows:

1. After the oxidation temperature reached 400 °C, the weight loss rate of the composites gradually increased with the prolongation of the oxidation time. After being oxidized at 500 °C for 9 h, the weight loss rate of the composites reached a maximum of 1.89 wt%.
2. After the high-temperature oxidation treatment of the composites, the damage of the carbon fiber was the most obvious, and the separation of the carbon fiber-SiC matrix interface was more obvious with the elevating of the oxidation temperature and the prolongation of the oxidation time.
3. As the oxidation time increased, the elastic modulus of the Al alloy matrix gradually

Figure 14 HRTEM micrographs of a cross-section of Al alloy–SiC matrix interface bonding area in the C_f/SiC–Al composites after oxidation at 500 °C for 9 h. **a** TEM micrograph, **b** Element mapping analysis of **(a)**, **c** HRTEM micrograph of the area enclosed by the purple square in **(a)**, **d** HRTEM micrograph of the area enclosed by the yellow square in **(c)**.



decreased, and the nanoindentation hardness hardly changed; when the oxidation temperature exceeded 400 °C, the elastic modulus and nanoindentation hardness of the SiC matrix decreased; and the elastic modulus and nanoindentation hardness of carbon fiber had little change.

- The in-plane compressive strength of the composites after oxidation treatment increased first and then decreased with the prolongation of oxidation time. After oxidizing at 400 °C for 7 h, the compressive strength reached the maximum value of 584.7 MPa; after oxidizing at 500 °C for 9 h, the compressive strength reached the minimum value of 347.8 MPa.

Acknowledgements

This research work was supported by the National Natural Science Foundation of China (Grant No. 92160202 and Grant No. U2167214), Postgraduate Research & Practice Innovation Program of Jiangsu Province (KYCX20_0197), and Priority Academic Program Development of Jiangsu Higher Education Institutions (PAPD).

Author contributions

JL: Conceptualization, Methodology, Investigation, Formal analysis, Visualization, Writing—original draft, Writing—review & editing, Funding acquisition. LY: Supervision, Project administration, Funding acquisition, Writing—review & editing. ZC: Supervision, Project administration, Funding acquisition. TG: Resources, Data Curation. TL: Methodology, Visualization, Resources.

Data availability

Data can be obtained by requesting the corresponding author.

Declarations

Conflict of interest The authors declare that they have no known competing financial interests or personal relationships that could have appeared to influence the work reported in this paper.

Ethical approval The experiment in this paper does not involve human tissue.

References

- [1] Qi LH, Ma YQ, Zhou JM, Hou XH, Li HJ (2015) Effect of fiber orientation on mechanical properties of 2D-C_f/Al composites by liquid-solid extrusion following Vacuum infiltration technique. *Mater Sci Eng A* 625:343–349
- [2] Zhou JM, Yuan MQ, Li Z, Meng HM, Zhang T, Qi LH (2019) A great improvement of tensile properties of C_f/AZ91D composite through grafting CNTs onto the surface of the carbon fibers. *Mater Sci Eng A* 762:138061
- [3] Ma YQ, Qi LH, Zheng WQ, Zhou JM, Ju LY (2013) Effect of specific pressure on fabrication of 2D-C_f/Al composite by vacuum and pressure infiltration. *Trans Nonferrous Met Soc China* 23:1915–1921
- [4] Li DG, Chen GQ, Jiang LT, Lin X, Wu GH (2015) Mechanical Property of M40J_p/5A06Al Composite at Elevated Temperatures. *Acta Metall Sin* 28:1175–1182
- [5] Xu ZG, Li DG, Wang PP, Jiang LT, Chen GQ, Wu GH (2021) Effect of TM (TM =Fe, Mn, Cr) alloying on the high temperature properties and strengthening mechanism of C_f/Al composites. *Compos B Eng* 211:108622
- [6] Hou LG, Cui C, Zhang JS (2010) Optimizing microstructures of hypereutectic Al-Si alloys with high Fe content via spray forming technique. *Mater Sci Eng A* 527:6400–6412
- [7] Kim JT, Soprunyuk V, Chawake N, Zheng YH, Spieckermann F, Hong SH, Kim KB, Eckert J (2020) Outstanding strengthening behavior and dynamic mechanical properties of *in-situ* Al-Al₃Ni composites by Cu addition. *Compos B Eng* 189:107891
- [8] Ezatpour HR, Sajjadi SA, Chaichi A, Ebrahimi GR (2017) Mechanical and microstructure properties of deformed Al-Al₂O₃ nanocomposite at elevated temperature. *J Mater Res* 32:1118–1128
- [9] Fei WD, Yue HY, Wang LD (2010) Equicohesive temperature of the interface and matrix and its effect on the tensile plasticity of Al₁₈B₄O₃₃ whiskers reinforced aluminum composite at elevated temperature. *Mater Chem Phys* 119:515–518
- [10] Saadallah S, Cablé A, Hamamda S, Chetehouna K, Sahli M, Boubertakh A, Revo S, Gascoin N (2018) Structural and thermal characterization of multiwall carbon nanotubes (MWCNTs) / aluminum (Al) nanocomposites. *Compos B Eng* 151:232–236
- [11] Zhong H, Wang Z, Zhou HJ, Ni DW, Kan YM, Ding YS, Dong SM (2017) Properties and microstructure evolution of C_f/SiC composites fabricated by polymer impregnation and pyrolysis (PIP) with liquid polycarbosilane. *Ceram Int* 43:7387–7392
- [12] Li BB, Liao JH, Chen ZF, Liu JB, Mao BX, Huang HQ, Yuan XS (2019) High-performance C_f/SiC composites with a novel needle-punched carbon fiber fabric fabricated by PIP process. *Mater Res Express* 6:115622
- [13] Uhlmann F, Wilhelmi C, Schmidt-Wimmer S, Beyer S, Badini C, Padovano E (2017) Preparation and characterization of ZrB₂ and TaC containing C_f/SiC composites via Polymer-Infiltration-Pyrolysis process. *J Eur Ceram Soc* 37:1955–1960
- [14] Liao JH, Chen ZF, Li BB, Liu JB, Guan TR, Yu SJ, Tang KY, Wu Q, Wang Y (2019) Microstructure and mechanical properties of C_f/SiC-Al composites fabricated by PIP and vacuum pressure infiltration processes. *J Alloys Compd* 803:934–941
- [15] Xue LP, Chen ZF, Liao JH, Xiao QQ, Li YH (2021) Compressive strength and damage mechanisms of 3D needle-punched C_f/SiC-Al composites. *J Alloys Compd* 853:156934
- [16] Snijders PC, Jeurgens LPH, Sloof WG (2002) Structure of thin aluminium-oxide films determined from valence band spectra measured using XPS. *Surf Sci* 496:97–109
- [17] Shin SE, Ko YJ, Bae DH (2016) Mechanical and thermal properties of nanocarbon-reinforced aluminum matrix composites at elevated temperatures. *Compos B Eng* 106:66–73
- [18] Sun Z, Shan ZD, Shao TM, Li JH, Wu XH (2021) A multiscale modeling for predicting the thermal expansion behaviors of 3D C/SiC composites considering porosity and fiber volume fraction. *Ceram Int* 47:7925–7936
- [19] Zhu JB, Wang YW, Bao CG, Lu BH (2021) Effect of oxidation of 3D-SiC preforms on the interfacial structure and mechanical properties of co-continuous SiC/Al composites. *Ceram Int* 47:14635–14646
- [20] Jia JH, Bai SX, Xiong DG, Chen Q, Li C, Gao MQ (2022) Microstructure and ablation behaviour of a C_f/SiC-Al composite prepared by infiltrating Al alloy into C_f/SiC. *J Alloy Compd* 895:162430
- [21] Ma Y, Wang S, Chen ZH (2010) Raman spectroscopy studies of the high-temperature evolution of the free carbon phase in polycarbosilane derived SiC ceramics. *Ceram Int* 36:2455–2459
- [22] Li Y, Xiao P, Zhou W, Luo H, Li Z (2018) Microstructure and properties of plain-weave carbon fabric reinforced ceramic composites containing Cu-Si alloy. *Compos B Eng* 145:129–135
- [23] Maleki K, Alizadeh A, Hajizamani M (2021) Compressive strength and wear properties of SiC/Al6061 composites reinforced with high contents of SiC fabricated by pressure-assisted infiltration. *Ceram Int* 47:2406–2413
- [24] Li LH, Zhang CY, Zhang C, Wang KJ, Bai H, Han D, Li M (2018) Compressive strength and damage mechanisms of 2D-C/SiC composites at high temperatures. *Ceram Int* 44:14026–14031

- [25] Suo T, Fan XL, Hu GL, Li YL, Tang ZB, Xue P (2013) Compressive behavior of C/SiC composites over a wide range of strain rates and temperatures. *Carbon* 62:481–492
- [26] Levin I, Brandon D (1998) Metastable alumina polymorphs: crystal structures and transition sequences. *J Am Ceram Soc* 81:1995–2012
- [27] Xiang Y, Cao F, Peng ZH, Wang Y, Li GD (2017) Evolution of microstructure and mechanical properties of PIP-C/SiC composites after high-temperature oxidation. *J Asian Ceram Soc* 5:370–376
- [28] Evertsson J, Bertram F, Zhang F, Rullik L, Merte LR, Shipilin M (2015) The thickness of native oxides on aluminum alloys and single crystals. *Appl Surf Sci* 349:826–832
- [29] Nakamura K, Sato Y, Takase T (2016) Analysis of oxidation behavior of vapor-grown carbon fiber (VGCF) under dry air. *Mater Lett* 180:302–304
- [30] Li B, Wang XY, Jin X, Li Q, Han B, Guo CJ (2022) Study on thermal damage properties of carbon fiber composite high-pressure hydrogen tank under fire scenarios. *Acta Energetica Solaris Sinica* 43:398–404
- [31] Huang JG, Guo LJ, Li KJ, Yan NN, Zhou L, Li YY (2021) Microstructures and oxidation behaviors of Al-modified and Al₂O₃-modified SiC coatings on carbon/carbon composites via pack cementation. *Ceram Int* 47:8105–8112
- [32] Urena A, Martinez EE, Rodrigo P, Gil L (2004) Oxidation treatments for SiC particles used as reinforcement in aluminium matrix composites. *Compos Sci Technol* 64:1843–1854
- [33] Liu GF, Chen TJ, Wang ZJ (2021) Effects of solid solution treatment on microstructure and mechanical properties of SiCp/2024 Al composite: a comparison with 2024 Al alloy. *Mater Sci Eng A* 817:141413
- [34] Dai JX, Sha JJ, Zu YF, Zhang ZF, Zhou X, Lei MK (2019) Microstructural tailoring and its influence on oxidation resistance of carbon fiber-reinforced C-SiC matrix composites. *Ceram Int* 45:2044–2052
- [35] Zhang Y, Zheng HL, Liu Y, Shi L, Xu RF, Tian XL (2014) Cluster-assisted nucleation of silicon phase in hypoeutectic Al-Si alloy with further inoculation. *Acta Mater* 70:162–173
- [36] Mandal D, Viswanathan S (2013) Effect of heat treatment on microstructure and interface of SiC particle reinforced 2124 Al matrix composite. *Mater Charact* 85:73–81

Publisher's Note Springer Nature remains neutral with regard to jurisdictional claims in published maps and institutional affiliations.

Springer Nature or its licensor (e.g. a society or other partner) holds exclusive rights to this article under a publishing agreement with the author(s) or other rightsholder(s); author self-archiving of the accepted manuscript version of this article is solely governed by the terms of such publishing agreement and applicable law.